Lung Nodule Growth Analysis from 3D CT Data with a Coupled Segmentation and Registration Framework

Yuanjie Zheng[1] Karl Steiner[2] Thomas Bauer[3] Jingyi Yu[1] Dinggang Shen[4]
Chandra Kambhamettu[1]
[1]Department of Computer and Information Sciences, University of Delaware, Newark, DE 19716
[2]Delaware Biotechnology Institute Delaware Technology Park, Newark, DE 19711
[3]Helen F. Graham Cancer Center Christiana Care Health Services, Newark, DE 19713
[4]Department of Radiology, University of Pennsylvania, Philadelphia, PA 19104

Abstract

In this paper we propose a new framework to simultaneously segment and register lung and tumor in serial CT data. Our method assumes nonrigid transformation on lung deformation and rigid structure on the tumor. We use the B-Spline-based nonrigid transformation to model the lung deformation while imposing rigid transformation on the tumor to preserve the volume and the shape of the tumor. In particular, we set the control points within the tumor to form a control mesh and thus assume the tumor region follows the same rigid transformation as the control mesh. For segmentation, we apply a 2D graph-cut algorithm on the 3D lung and tumor datasets. By iteratively performing segmentation and registration, our method achieves highly accurate segmentation and registration on serial CT data. Finally, since our method eliminates the possible volume variations of the tumor during registration, we can further estimate accurately the tumor growth, an important evidence in lung cancer diagnosis. Initial experiments on five sets of patients' serial CT data show that our method is robust and reliable.

1. Introduction

Lung cancer is the fist most common cause of cancer death in men, and the second most common cause in women, according to the 2004 world health report of the World Health Organization (WHO). It causes 1.3 million annual deaths worldwide in 2006. Early detection of lung cancer can significantly improve the long-term health of those diagnosed with it. Methods that allow early detection of lung cancer, such as the helical low-dose CT (Computed Tomography) scan, x-ray, and bronchoscopy, are of value in the identification of incurable metastatic cancer, as well as small cancer that can be cured by surgical resection and prevention of widespread. Since the late 1990s, there has been a great deal of interest in using helical CT as the primary screening modality for lung cancer detection, due to its affordable cost and high-resolution.

A patient who presents abnormality on CT scans can be diagnosed with lung cancer, or other nonmalignant diseases like tuberculosis, pneumonia, or sarcoidosis, etc. Growth patterns of lung abnormality in serial CT images have been proven to be a significant indicator of lung cancer. If a growth of 1cm or larger is detected for a lung nodule smaller than 3cm, this nodule is at a high risk of developing lung cancer [4]. On the other hand, a nodule that has not demonstrated an increase in diameter during a follow-up period of 2 years is almost certainly non-cancerous [3].

Computer-aided diagnosis (CAD) with CT data [10, 5, 2] can increase the radiologist's efficacy and provide more accurate diagnosis for lung cancer. Such procedures often consist of segmentation of CT scan of lung, and intrapulmonary structures, identification of nodule candidates, and registration of serial images, etc. Registration aligns two images scanned at different times spatially, while segmentation specifies the spatial domain of nodule or lung. Accurate registration and segmentation leads to accurate computation of nodule growth [9, 6]. Therefore, CAD techniques are also important in detecting and measuring nodule growth.

There are multiple challenges in both registration and segmentation of serial lung CT data. *First*, for Ground Glass Opacity (GGO) nodules, the low contrast and fuzzy margins make accurate segmentation of GGO very hard. *Second*, the usually long duration (one year for example) and the different conditions between two sets of CT scans cause large nonrigid deformation of lung, and intensity differences within the same tissue. Both of these create problems for accurate registration and segmentation. *Third*, the large data size of high-resolution CT scanning can cause problems for 3D registration or 3D segmentation, due to the need of significant memory and computational resources. *Fourth*, general nonrigid registration may change not only the shape but also the volume of lung tumors, because of

the possibly large nonrigid deformation of the lung in serial data, as well as the higher similarity between intensities of the same nodule before and after growth (see Fig. 1). Similar phenomena have been reported in the literature when measuring breast tumors in Magnetic Resonance Imaging (MRI) [13]. It is worth noting that changing the shape and the volume of lung tumor due to inaccurate registration might lead to significant errors to the measurement of tumor growth.

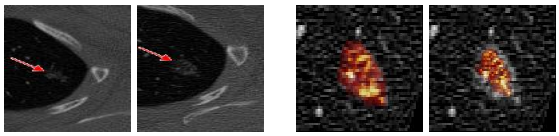

(a) (b) (c) (d)

Figure 1. Demonstration of importance of using rigid transformation to align same tumor in serial lung CT data. (a) A small tumor detected during the initial CT scan. (b) A larger tumor detected during a follow-up CT scan. (c) The overlapping result of a nonrigidly aligned small tumor and the large tumor. (d) The overlapping result of the rigidly aligned small tumor and the large tumor.

In this paper, we propose a new framework to simultaneously segment and register lung and tumor in serial data. Our method assumes non-rigid transformation for lung deformation and rigid structure for the tumor, to preserve the volume and the shape of the tumor during the registration. For segmentation, we apply a 2D graph-cut algorithm on the 3D lung and tumor. For registration, we use a B-Spline-based nonrigid transformation [12][11] to model the lung deformation, while imposing rigid transformation on the tumor by setting the control points within the tumor to form a control mesh. We then simultaneously compute the segmentation and registration via a joint optimization. Such a joint optimization has been shown in the literature to have better performance than computing the segmentation and registration independently [16, 14]. We also observe that more accurate segmentation and registration of lung and tumor can be obtained using our algorithm.

The key contribution of our method can be summarized as follows. (1) It is the first attempt where two different transformations are applied on a tumor and a lung in CAD of lung cancer, i.e., a rigid transformation on the tumor and a nonrigid deformation on the lung. (2) It is simple and efficient for integrating rigid and nonrigid transformations. (3) It solves the segmentation and registration simultaneously in a joint optimization framework.

2. Problem Statement and Algorithm Overview

Given two volumes V_1 and V_2 of serial lung CT data, which are respectively scanned before and after the nodule's growth, our goal is to find the correspondence mapping $\mathcal{T}$ that warps every voxel in the lung of V_1 to the space of V_2, as well as to find the segmentation S of lungs and nodules. Here, $\mathcal{S} = \{\mathcal{S}_{l1}, \mathcal{S}_{l2}, \mathcal{S}_{n1}, \mathcal{S}_{n2}\}$ represents lungs' and nodules' segmentation in V_1 and V_2, respectively. The tumor growth can be computed from the nodules' segmentations $\mathcal{S}_{n1}$ and $\mathcal{S}_{n2}$.

The transformation $\mathcal{T}$ consists of a global transformation $\mathcal{T}_g$ and a local transformation $\mathcal{T}_l$, i.e.,

$$\mathcal{T} = \mathcal{T}_g + \mathcal{T}_l. \tag{1}$$

The global transformation will be computed first in a general way by minimizing the dissimilarity measure between the transformed volume of V_1 and V_2. After that, we compute volume V_1' by employing the estimation of T_g on V_1.

We cast the estimation of local transformation as a *maximum a posteriori* (MAP) estimation of T_l and S, given V_1' and V_2, as in [16], i.e.,

$$T_l, S = \arg\max_{T_l, S} \mathcal{P}(T_l, S | V_1', V_2). \tag{2}$$

A two-step optimization algorithm similar to [16] is applied to solve this equation (2):

1. Segment the lungs and nodules in V_1' as initial estimate S' of S.
2. Repeat the following steps until convergence:
   (a) Compute $T_l' = \arg\max_{T_l} \mathcal{P}(T_l | S', V_1', V_2)$
   (b) Compute $S' = \arg\max_{S} \mathcal{P}(S | T_l', V_1', V_2)$

We need to note that S contains segmentations of the lung, nodule and other tissues, and T_l is the integration of the rigid transformation on nodule, T_{l_r}, and the nonrigid deformation on lung, T_{l_n}.

The global transformation is represented by a rigid model, which is determined by rotations α, β, and γ and translations δ_x, δ_y and δ_z relative to axis x, y, and z, respectively. The parameters in the model are estimated by minimizing the Sum of Squared Differences (SSD) between the globally transformed volume of V_1 and V_2. Gradient decent optimization can be used to get a local minimum, which is enough for aligning the volumes globally.

The local transformation is represented by the integration of rigid transformation on nodule, T_{l_r}, and nonrigid transformation on lung, T_{l_n}, in which the latter is represented by a B-spline based free-form deformation (FFD) [12].

The segmentation of 3D lung and tumor is accomplished by using a graph-cut [15] based 2D segmentation algorithm. The estimation of local transformation and segmentation of nodule, lung and other tissues are performed simultaneously by interleaving them. They can benefit from each other, and more accurate results can therefore be produced.

3. Registration Using Segmentations of Lung and Nodule

This section describes the details of step 2(a) in the optimization algorithm of equation (2).

We use nonrigid registration for the lung to account for its complicated deformation, and at the same time treat lung nodule as a rigid structure. Our approach has several advantages: *First*, shape and volume of nodule in registration will be preserved; *Second*, the lung deformation can be effectively represented using nonrigid deformation; *Third*, the nodule's position can be mapped accurately from V_1' to V_2 because of the guiding of nonrigid registration of the lung during the registration process. All of the advantages can lead to higher accuracy in nodule growth computation.

A number of methods can be found related to embedding rigid structures in the nonrigid deformation field during the registration process. They can be classified into three methods. The *first* method is based on point interpolation technique together with a weighting of the deformation according to a distance function [8]. The *second* method is based on the fact that the Jacobian matrix at a location is orthogonal if its transformation is locally rigid [7], or the determinant of Jacobian matrix is equal to one if it is locally incompressible [11]. The *third* method enforces coupled control points having the same displacements [13], in which only the control points related to the rigid structure are coupled. We note that in [13] the transformation of the whole volume is composed of a global transformation and local deformation, and the rotations of the rigid structures are assumed to be totally accounted for in the global rigid transformation, i.e., there are only displacements and no rotations for the coupled control points. Our approach is closer to the third kind of methods of integrating rigid structure in nonrigid registration, which will be detailed below. In particular, the differences between the method in [13] and our method will be extensively compared in the end of Section 3.2.

3.1. Transformation Models

We use the same rigid transformation model for the segmented nodule, as the global transformation model explained in section 2.

For the local deformation of lung, we use the B-spline based FFD [12]. The FFD can be written as the 3-D tensor product of 1-D cubic B-splines as follows

$$T_{l_n}(x,y,z) = \sum_{h=0}^{3}\sum_{m=0}^{3}\sum_{n=0}^{3} B_h(u)B_m(v)B_n(w)\phi_{i+h,j+m,k+n} \qquad (3)$$

where ϕ denotes mesh of control points, i, j, and k denote the indices of the left-upper-rearer most control point of the $4 \times 4 \times 4$ control points around (x, y, z) for interpolation, B_h represents the hth B-spline basis function. More details related to the specification of (i, j, k) and expressions of the B-spline basis functions are referred to [12].

3.2. Integration of the Rigid and Nonrigid Transformations

The integration of rigid transformation of the segmented nodule and nonrigid transformation of lung is used to represent the local transformation from V_1' and V_2, in order to keep the volume and shape of nodule in V_1' unchanged while attaining high alignment accuracy during the process of registration.

To do so, we use four techniques. *First*, the control points which are located in the domain of the segmented nodule are coupled, and the same rigid transformation is assumed for them. *Second*, the transformation of voxels in the segmented nodule is obtained directly by using the current estimated rigid transformation matrix, instead of interpolating the related control points. *Third*, transformations of the voxels not in the nodule will be computed by interpolation of control points' motions as in equation (3). Note that some of the coupled control points are possibly used in interpolation. Their motions are computed directly with the rigid transformation matrix currently estimated for nodule. *Finally*, a regularization term is added to impose smoothness in transformation.

We also keep most of the control points in the background fixed, and move only the control points in the smallest bounding box of the currently segmented lung plus two control points along each direction outside the box, in order to save computational time, as shown in Fig. 2. In addition, only the voxels within the box larger than the smallest bounding box for half precision of control points along each direction (denoted as the space by Ω_1), i.e. the area within the yellow rectangle in Fig. 2, will be transformed in order to save computational time.

Our method differs with [13] in several ways. *First*, we enforce a same rigid transformation on the coupled control points, while the same displacements are imposed on the coupled control points in [13]. Our method can fit better for the case when the rotation of the rigid structure can not be represented very well by the global rigid transformation T_g. *Second*, only the control points in the domain of the rigid structure are coupled in our method, and are enforced by rigid transformation. In [13], more control points adjacent to, but outside, the smallest bounding box of the rigid structure are also coupled in order to guarantee the rigid transformation of the rigid structure, and thus possibly more voxels than the rigid structure will be set tobe rigid, as shown in Fig. 2. In addition, [13] assumes the coupled control points not in the rigid structure have the same displacements to the ones in the rigid structure. The assumption is often violated especially when the former ones are transformed nonrigidly

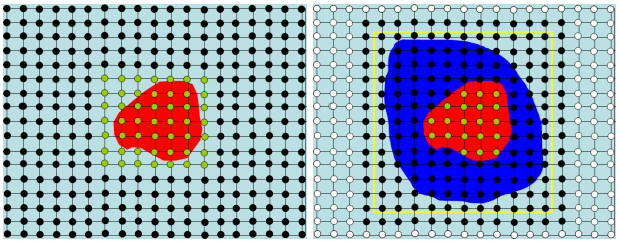

Tanner's method Our method

Figure 2. Differences between Tanner's method [13] and our method in integrating rigid and nonrigid transformations during registration. 2D case is shown. Red regions indicate rigid structure (tumor), blue regions denote nonrigid structure (lung), green filled circles are coupled control points, black filled circles are uncoupled control points which can move freely, white filled circles are fixed control points, and the yellow rectangle shows the region in which the pixels (in 3D case: voxels) need to be transformed and used to compute dissimilarities in registration of our method.

by the lung's deformation. We relax the control points adjacent to the rigid structure from rigid to nonrigid transformation, thus their motions can be more accurately estimated. This can also bring better results for control points within the rigid structure, because of their mutual influences by the smoothing term for transformation in registration. *Finally*, in our method, voxels in the rigid structure of V_1' are transformed directly with the estimated rigid transformation matrix to V_2, and other voxels are interpolated with the corresponding control points' motions, while in the methods of [13], all of the voxels are transformed by interpolating the control points.

3.3. Dissimilarity Measure, Smoothness Constraints, and Optimization

The main part of lung registration is to find an optimal smooth transformation T_l' which can transform V_1' to best match with V_2. Mathematically, the optimization in step 2(a) of equation (2) can be formulated in more details as follows:

$$T_l' = \arg\min_{T_l \in \Gamma} [dis(V_2, V_1'') + reg(T_l)] \tag{4}$$

where $V_1'' = V_1' \circ T_l$ means the transformed volume of V_1' by T_l, Γ denotes the space of transformations integrating rigid transformation on nodule and nonrigid transformation on lung, $dis()$ means the dissimilarity measure of the two volumes, and $reg()$ denotes a regularization term which is used to enforce smoothness on the transformation field.

The dissimilarity measure in equation (4) is defined as the sum of the squared difference between intensity vectors and mean intensity vector of corresponding class, as given next:

$$dis(V_2, V_1'') = \sum_{i \in \Omega_1} w_{c_i} ||\vec{I}(i) - \vec{\mu}_{c_i}||^2 \tag{5}$$

where $\vec{I}(i)$ is the 2-component intensity vector of voxel i in domain Ω_1, which is composed of intensities of the voxel in V_1'' and V_2, respectively, $\vec{\mu}_{c_i}$ denotes the mean intensity vector of the segmentation class c_i of voxel i, $||\cdot||$ means $L2$-norm, and w_{c_i} is the weight value assigned to voxels of class c_i.

The regularization term in equation (4) is computed as

$$reg(T_l) = \sum_{(x,y,z) \in \Omega_1} (T_{lxx} + T_{lyy} + T_{lzz} + 2T_{lxy} + 2T_{lxz} + 2T_{lyz}) \tag{6}$$

where T_{lxx}, T_{lyy}, T_{lzz}, T_{lxy},T_{lxz}, and T_{lyz} are the squared second order derivative of the transformations.

4. Segmentation of Lung and Nodule Using Registration

This section describes step 2(b) in the optimization algorithm of equation (2).

We show the segmentations of lung and nodule will be more accurate based on both V_1'' and V_2 simultaneously rather than independently, because more information is used during the process of segmentation. After a new iteration of the registration, we get the voxels' updated correspondences between V_1' and V_2, which are usually better optimized. The accurate estimation of correspondences can help improve the segmentation.

The segmentations of 3D lung and nodule are performed by using a graph-cut based 2D image segmentation algorithm [15]. The 2D image segmentation algorithm runs within a rectangle region around the initialized lung or nodule, which is always 20 pixels larger for the lung, or 10 pixels larger for the nodule, compared to the respective smallest bounding box. For the nodule, the bounding box is set as the combination of tentatively segmented regions of both small and large nodules in two serial data. The middle slice will be first segmented by taking the segmentation in the last iteration as initialization, and then the result is propagated to the nearest unsegmented neighbor slices as the initialization for graph-cut based segmentation. The process of propagating the segmentation to neighboring slices will stop once the segmented area in a particular slice is below a certain threshold, such as 10 pixels used for our experiments.

For the 2D segmentation of one slice, the similarity of intensities in the same class, the spatial smoothness of class labels, the requirement of segmented boundaries being close to the high gradient locations, as well as the requirement of segmented boundaries to be close to the boundaries segmented in the neighboring slices are all considered, to improve the segmentation accuracy.

The segmentation in one slice is performed by minimizing the following energy function with graph-cut algorithm.

$$E = \sum_{i \in \Omega_1'} E_1(c_i) + \lambda_1 \sum_{<i,j> \in \mathcal{N}} E_2(c_i, c_j) + \lambda_2 \sum_{<i,j> \in \mathcal{N}_d} E_3(c_i, c_j) + \lambda_3 \sum_{<i,j> \in \mathcal{N}_{l|n}} E_4(c_i, c_j) \quad (7)$$

where factors λ_1, λ_2 and λ_3 are used to adjust the relative importance of the four energy terms, Ω_1' is the domain to be segmented in the image, $\mathcal{N}$ are the neighbor voxels (4 nearest neighbors in 2D space are used in our experiments), $\mathcal{N}_d$ means voxels pair having different segmentation classes, $\mathcal{N}_{l|n}$ means voxels pair having different segmentation classes, where one class is either lung or nodule.

E_1 is used to ensure similarities of intensities in one class. A Gaussian distribution is assumed for the 2-components intensity vectors (composed of the intensity values in V_1'' and V_2) in each class l, and Gaussian model is estimated based on the intensity vectors of currently specified pixels in this class. Thus, E_1 is specifically defined as

$$E_1(c_i) = 1 - Pr\left(\vec{I}(i) | \vec{\mu}_{c_i}, \vec{\sigma}_{c_i}\right). \quad (8)$$

where the latter term measures the probability of the intensity vector $\vec{I}_i$ of pixel i belonging to class c_i. The class c_i is represented by a Gaussian model with mean $\vec{\mu}_{c_i}$ and variance $\vec{\sigma}_{c_i}$.

$E_2(c_i, c_j)$ is used for imposing the spatial smoothness of segmentation, which is simply defined as follows:

$$E_2(c_i, c_j) = 1 - \delta(c_i - c_j) \quad (9)$$

where δ is a Kronecker delta function.

E_3 obliges the segmentation boundary to locate at places with high intensity changes, which is defined as follows:

$$E_3(c_i, c_j) = g\left(\|\vec{I}(i) - \vec{I}(j)\|\right) \quad (10)$$

where the function g is defined as:

$$g(\zeta) = \frac{1}{\zeta + 1}. \quad (11)$$

E_4 prevents the segmented boundary from being too far from the one of the nearest neighbor slice, which is defined as

$$E_4(c_i, c_j) = 1 - g\left(\beta \cdot D_{i,j}\right) \quad (12)$$

where $D_{i,j}$ is the distance from the center point between pixel i and pixel j to the boundary of initialized segmentation, i.e., the obtained segmentation of the nearest neighbor slice, and β is a control parameter for $D_{i,j}$. Note that for 2D segmentation of the starting slice, E_4 will not be considered.

For the starting slice's initial segmentations, we first manually segment lung and nodule, second, specify Ω_1' which is the corresponding domain in one slice of Ω_1 shown as yellow rectangle in Fig. 2, third, manually classify the segmented lung into lung and interior structures and the area outside the lung within Ω_1' into 3 classes with K-Means algorithm, and finally, use the graph-cut algorithm to refine the segmentation by minimizing the energy function in equation 7.

Different classes are set for pixels in the bounding boxes of lung and nodule, respectively, for better segmentation. For the lung, 3 classes are set. For a nodule, it is more complicated due to tumor growth and possible inaccurate alignment between small and large tumors. To achieve better results, we set four classes for the voxels within the bounding box that includes both temporarily segmented small and large tumors. The four classes represent (1) pulmonary voxels for both the volumes, (2) voxels of nodule for V_1'' while lung for V_2, (3) voxels of nodule for both the volumes, and (4) voxels of lung for V_1'' while nodule for V_2. Some classes might be eliminated or added during the evolution of simultaneous segmentation and registration process. For example, the second class should be removed once a small nodule is aligned completely within the large nodule. We note that here we use knowledge that the intensities of nodule are always higher than pulmonary voxels. After the convergence of the segmentation algorithm, the combination of the second and third class are treated as small nodule, and the combination of the third and the fourth class are a large nodule. After finishing segmentation of each slice with graph-cut, morphological closing and hole filling operations are used to fill possible unexpected holes in the segmented regions.

One more thing needs to be noted for the optimization algorithm related to equation (2). For a nodule, the dissimilarity measure expressed by equation (5) and the energy term E_1 determined by equation (8) can be low even when the small nodule is aligned wrongly to lung parenchyma considering the possible homogenous intensities for the segmented tumor and lung parenchyma. The wrong alignment can occur due to the small volume of the nodule and possibly large deformation of the lung. To deal with this problem, we set a high weight value, e.g. 1, for the nodule, while very low weight, e.g. 0.1, for the remaining part at the first iteration. Note that the initial segmentations of the nodule for the repetitive optimizations are supposed as correct in terms of location, although the accuracy of nodule's spatial extent might be not so high. Thus, the use of high weight for the nodule can guarantee that the small nodule is aligned in the large nodule at the beginning of the repetition. Gradually, the difference of weights on nodule and other parts can be eliminated with the evolution of the registration.

5. Experimental Results

In our experiments, we use the CT volumes acquired with a Spiral high resolution CT scanner. Our simultaneous segmentation and registration scheme was tested on 6 volumes of 3 patients, in which 2 volumes of each patient were scanned with time interval of about 12 months. The size of each volume is $512 \times 512 \times 331$ pixels, and the voxel size is $0.54 \times 0.54 \times 1.0\, mm^3$.

We have performed three experiments to show (1) the necessity of the usage of nonrigid deformation for lung's registration, (2) the improvement of registration and segmentation by interleaving them, and (3) the improvement of tumor growth computation by enforcing rigid structure for the segmented nodule while enforcing a nonrigid transformation for lung.

5.1. Necessity of using Nonrigid Deformation for Lung's Registration

The lung's deformation is usually far more complicated than a rigid transformation. This is also true for our data sets. The long duration between the two lung scans and the possibly different scanning parameters at inhalation or exhalation can complicate the lung's transformations.

The assumption of nonrigid transformation, other than rigid transformation, of lung has improved the accuracy of alignment, which can be seen in experimental results on one of our subjects as shown in Fig. 3. The initial volume is registered with the follow-up scan volume in our experiments.

Removal of the global rigid transformation has also helped roughly align the two volumes. It can be confirmed by comparing the overlapping results in Fig. 3 (a) and (b), before and after applying rigid transformation. The rigid transformation was computed on the whole volume without any tissue segmentation. Note that the lungs in the two volumes were manually segmented before performing the global transformation.

Besides the alignment effect by the global rigid transformation from Fig. 3, we can also see from Fig.3 (b) that the lung in the initial volume is smaller than the second one. This are mainly caused by the fact that the initial volume was scanned closer to inhalation while the follow-up scan volume was scanned closer to exhalation. Therefore, nonrigid transformation is necessary for aligning these two lungs accurately.

The improvement by nonrigid transformation in registration can be observed from the overlapping result in Fig. 3 (d) and (f), compared to the case of using only rigid transformation in Fig. 3 (c) and (e). In particular, interior structures of the lung are aligned better after using nonrigid transformation.

To better show the improvement of alignment by nonrigid transformation over rigid transformation, we also

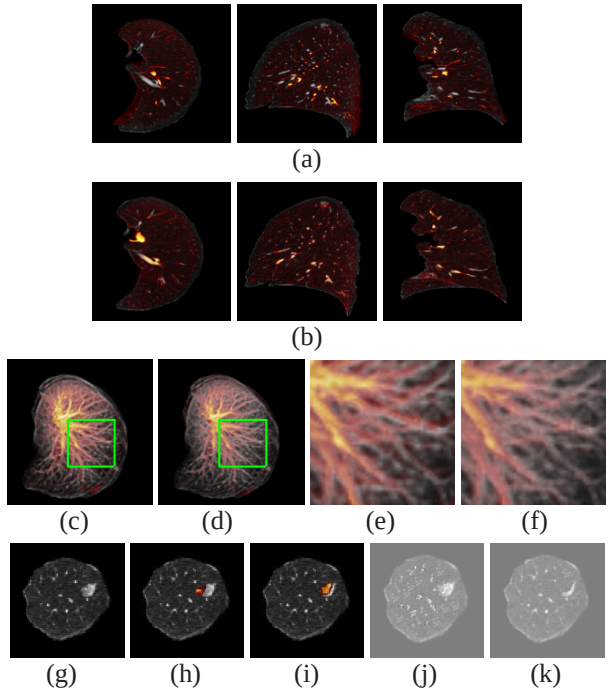

Figure 3. Comparisons between global rigid and local nonrigid transformations on lung data. (a) and (b) are the overlapping results of the same lung in initial volume (red) and in the follow-up scanned volume (grey), before and after applying global rigid transformation, respectively. For both (a) and (b), the panels from left to right are the transverse, coronal and sagittal views, respectively. (c) and (d) are respectively the rendering results of the rigidly transformed lung, and the nonrigidly transformed lung after removing rigid transformation. The parts within green rectangles are shown in (e) and (f) respectively. (g) is the lung and nodule in the follow-up scan volume. (h) and (i) are the overlapping results of segmented initial nodule on the follow-up scan lung in (g), aligned by rigid transformation and nonrigid transformation, respectively. For (c), (d), (e), (f), (h) and (i), red color corresponds to the early-time volume and grey to the later-time volume. (j) and (k) are the difference maps of the aligned initial lung with the follow-up scan lung, by rigid transformation and nonrigid transformation, respectively.

show the overlapping results of the transformed initial nodules on the follow-up scan volume, as shown in Fig. 3 (h) and (i). Using rigid transformation only (Fig. 3 (h)), the initial nodule was not even aligned to the region of grown nodule in the follow-up scan volume. Alignment is improved by using nonrigid transformation, as shown in Fig. 3 (i). However, we notice that there is an about $8mm^3$ volume change on the initial nodule after nonrigid transformation, which indicates the necessity of using the rigid structure to constrain the deformation in nodule as proposed in this paper.

Fig. 3 (h) and (i) show the difference maps between the aligned, initially scanned lung and the follow-up scan lung using global rigid transformation and nonrigid transformation, respectively. It can be observed that alignment errors

by nonrigid transformation are obviously smaller than those by rigid transformation.

5.2. Improvement of Registration and Segmentation by Coupling them

Next, we demonstrate the registration improvement through the difference maps of the first iteration and the third iteration between the transformed image and the target image, by coupling the registration and segmentation with the optimization algorithm in section 2, as shown in Fig. 4.

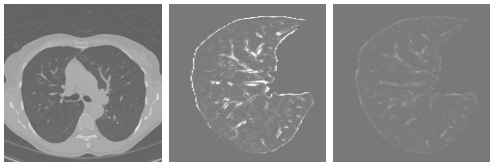

(a) (b) (c)

Figure 4. Improvement in registration by segmentation. (a) One slice of the follow-up scan CT volume of lung. (b) and (c) are the intensity difference maps between the transformed initial scan volume and the follow-up scan volume in the 1st and the 3rd iteration, respectively.

Note that, as shown in Fig. 4 (b), the inaccurate segmentation leads to large registration error. With better segmentation, the registration error is decreased as shown in Fig. 4 (c). Although a general nonrigid registration algorithm might result in a better difference map, compared to Fig. 4 (c), the volume and the shape of the nodule in the initial scan volume might be changed a lot due to high nonrigid registration.

To quantitatively evaluate the performance of our algorithm on segmentation, we measure the distance between automatic segmented boundaries of lung tumors and manual segmentation (similar to [1]). Based on all our testing samples, the mean error of boundary distances is 3.50 pixels.

5.3. Improvement of Tumor Growth Computation

When registering the initial scan volume to the follow-up scan volume, the volume and shape of nodule in the initial scan volume can be changed due to the following four factors if no rigid constraint is placed on nodule: the lung's transformation, the precision of control points used in B-Spline based registration, the size of the nodule, and the actual tumor growth between the two data sets. These factors are explained next one by one. *First*, larger degree of lung's transformation between the two datasets can bring in more errors to the computation of the nodule's volume. *Second*, more dense control points possibly lead to larger changes to nodule's volume. With more control points in the nodule, changes of the nodule's volume come not only from the deformation of the lung, but also the nonrigid mapping from one nodule to the other as shown in Fig. 1. *Third*, larger size

Resolution	50	30	20	10	5
subject1	13.5	13.3	13.5	20.9	34.7
subject2	6.8	6.3	6.3	19.6	29.5

Table 1. Changes (in percentage) of nodule volume with respect to the use of different density of control points in B-Spline, when applying nonrigid registration on the lung without enforcing a rigid structure for the nodule. The density value, e.g., 50, relates to the resolution of the control points is $50 \times 50 \times 50 mm^3$. The nodules sizes are $21.2 \times 21.4 \times 20.6 mm^3$ for subject1, and $15.4 \times 14.9 \times 19.2 mm^3$ for subject2.

of a nodule might mean larger changes in nodule volume in nonrigid registration due to a larger nodule can contain more control points of the B-Spline. *Finally*, a larger real nodule growth might bring larger changes to nodule's volume in registration since the deference in nodule of different times is large.

Our algorithm enforces rigid structure to the nodule, and therefore, changes to the nodule's volume by our registration method only come from errors in segmentation, which is proven to be very low by experiments. To show the merits of our algorithm on the tumor growth computation, we demonstrate in Table 1 the percentage of nodule volume change under nonrigid transformation, with respect to the use of different density of control points in B-Splines. Note that manual segmentation of nodules by a well trained rater is used as ground-truth. Based on our experiments, the mean and variance of percentages of the nodule volume variations with our algorithm, caused by errors in segmentation, are 0.8 and 0.6.

Some overlapping results after our segmentation and registration are also shown in Fig. 5. It can be observed that the nonlinear mappings from the initial scan nodule to the second scan nodule are accurate, and thus the automatic measurement of the nodule's growth property become possible. Note that, if the nodules are not well aligned, we can only compute the volume changes, while the different growth properties of nodule in different directions cannot be obtained, even after we get the accurate segmentations for nodules.

Finally, we also provide the rendering results of a lung and a nodule segmented using our method in Fig. 6. The rendering results for the nodule looks blurred due to its small size.

6. Conclusions and Future Work

We have presented a new framework to simultaneously segment and register a lung and a tumor in serial CT data. Our method assumes the nonrigid transformation for lung deformation and the rigid structure for tumor. We have used a B-Spline-based nonrigid transformation to model the lung deformation, while enforcing the rigid transformation

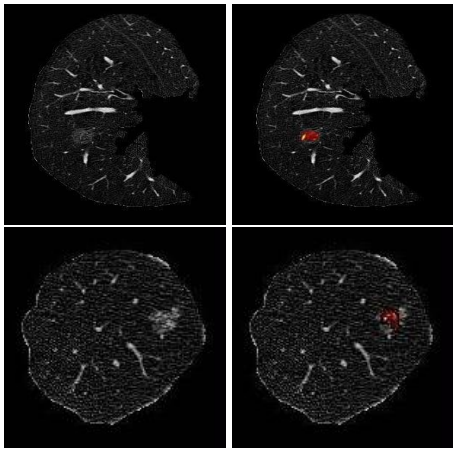

Figure 5. Overlapping results of our aligned initial scan nodule with the follow-up scan volume. The left column shows the segmented lung in the follow-up scan volume, while the right column shows the corresponding overlapping results.

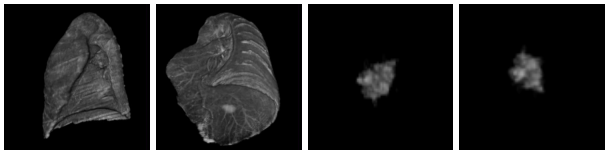

Figure 6. Volume renderings of a lung and a nodule segmented by our method. Two views are displayed for both lung and nodule.

on the tumor to preserve both volume and shape of the tumor. For segmentation, we have applied a 2D graph-cut algorithm on the lung and tumor. For registration, we set the control points within the tumor to form a control mesh and enforce the tumor region to follow the same rigid transformation as the control mesh. By allowing nonrigid registration for the lung and rigid registration only for the tumor, the tumor volume and shape can be preserved during registration, thus increasing the accuracy of measuring tumor volume growth as well as tumor growth patterns.

In the future, we plan to design the special features, other than intensity, for the segmentation of GGO tumors. GGO-tumor voxels have a hazy appearance within the tumor, thus, the classical intensity-based segmentation methods may fail. We also plan to design a system for lung cancer diagnosis by computing the volume changes of the nodule as well as the different growth patterns, according to the registration and segmentation results. Finally, tumor growth can be more accurately estimated, if the inflation and deflation of lung can be obtained and used in registration. In this case, we might also be able to model the change of nodule volume due to the inflation and deflation of lung.

7. Acknowledgement

This publication was made possible by Grant Number 2 P20 RR016472-07 under the INBRE program of the National Center for Research Resources (NCRR), a component of the National Institutes of Health (NIH).

References

[1] Y. S. Akgul and C. Kambhamettu. A coarse-to-fine deformable contour optimization framework. *IEEE Trans. Pattern Anal. Mach. Intell.*, 25(2):174–186, 2003. 7

[2] K. Awai and et al. Pulmonary nodules at chest CT: Effect of computer-aided diagnosis on radiologists detection performance. *Radiology*, 230:347–352, 2004. 1

[3] C. A. Good and T. W. Wilson. The solitary circumscribed pulmonary nodule: study of 705 cases encountered roentgenologically in a period of three and one-half years. *J. Am. Med. Assoc.*, 166:210–215, 1958. 1

[4] S. G. Jenning and et al. Lung tumor growth: assessment with CT-comparison of diameter and cross-sectional area with volume measurements. *Radiology*, 231(3):866–871, 2004. 1

[5] K. G. Kim and et al. Computer-aided diagnosis of localized ground-glass opacity in the lung at CT: Initial experience. *Radiology*, 237:657–661, 2005. 1

[6] W. J. Kostis and et al. Three-dimensional segmentation and growth-rate estimation of small pulmonary nodules in helical ct images. *IEEE Trans. Med. Img.*, 22(10):1259–1273, 2003. 1

[7] D. Loeckx and et al. Nonrigid image registration using free-form deformations with a locally rigidity constraint, 2004. MICCAI. 3

[8] A. Moreno and et al. Non-linear registration between 3d images including rigid objects: Application to CT and PET lung images with tumors, 2006. In Workshop on Image Registration in Deformable Environments, DEFORM 2006. 3

[9] A. P. Reeves and et al. On measuring the change in size of pulmonary nodules. *IEEE Trans. Med. Img.*, 25(4):435–450, 2006. 1

[10] A. P. Reeves and W. J. Kostis. Computer-aided diagnosis for lung cancer. *Radiol. Clin. North Am.*, 38(3):497–509, 2000. 1

[11] T. Rohlfing and J. C. R. Maurer. Nonrigid image registration in shared-memory multiprocessor environments with application to brains, breasts, and bees. *IEEE Trans. Infor. Tech. In Biomedicine*, 7(1):16–25, 2003. 2, 3

[12] D. Rueckert and et al. Nonrigid registration using free-form deformations: Application to breast MR images. *IEEE Trans. Med. Imag.*, 18:712–721, 1999. 2, 3

[13] C. Tanner and et al. Volume and shape preservation of enhancing lesions when applying non-rigid registration to a time series of contrast enhancing MR breast images, 2000. MICCAI. 2, 3, 4

[14] A. Yezzi and et al. A variational framework for joint segmentation and registration, 2001. MMBIA. 2

[15] R. Zabih and V. Kolmogorov. Spatially coherent clustering using graph cuts, 2004. CVPR'04. 2, 4

[16] Y. Zheng and et al. De-enhancing the dynamic contrast-enhanced breast mri for robust registration, 2007. MICCAI. 2